

New Time-Domain Line Protection Principles and Implementation

E. O. Schweitzer, III, B. Kasztenny, M. Mynam, A. Guzmán, and V. Skendzic
Schweitzer Engineering Laboratories, Inc.

Presented at the
8th Annual Protection, Automation and Control World Conference
Wroclaw, Poland
June 27–29, 2017

Originally presented at the
13th International Conference on Developments in Power System Protection, March 2016

New time-domain line protection principles and implementation

E. O. Schweitzer, III, B. Kasztenny, M. Mynam, A. Guzmán, V. Skendzic

*Schweitzer Engineering Laboratories, Inc., 2350 NE Hopkins Court, Pullman, WA 99163 USA,
venkat_mynam@selinc.com*

Keywords: Line protection, traveling waves, incremental quantities, differential protection, distance protection.

Abstract

Since electric power's earliest days, engineers have continually improved protection as measured by safety, speed, security, and dependability. The quest for faster fault clearing is more relevant today than ever. This paper reviews new time-domain line protection operating principles using traveling waves and incremental quantities. We discuss operating principles of novel directional and differential elements based on traveling waves and Zone 1 distance and directional elements based on incremental quantities. This paper provides details on the actual implementation of these principles in a high-performance relay platform and shares performance results from simulations and field recordings.

1 Introduction

Today, time-domain relays are becoming available for ultra-high-speed line protection. These relays use traveling-wave (TW) principles as well as tried-and-true incremental-quantity principles to provide ultra-high-speed and secure line protection. High sampling rates, data storage, processing power, and communications capabilities of new relay hardware platforms allow us to improve line protection operating times [1] and fault locating [2].

Section 2 of this paper briefly reviews the data acquisition and signal processing associated with implementing the time-domain line protection elements. Section 3 discusses the operating principles of TW-based line protection elements: TW32 directional element and TW87 differential element. Section 4 briefly discusses the operating principles of incremental quantity elements: TD32 directional element and Zone 1 underreaching TD21 distance element. Section 5 illustrates the performance of TW32 and TW87 using digital simulations. We also use a field case captured by the TW fault locator to show the performance of the TW87 element. We provide a more detailed description of the elements and their performance in [3].

2 Data acquisition and signal processing

This section summarizes the data acquisition and signal processing for the time-domain line protection elements. We start by listing key signals and settings common to our line protection elements.

- v_Φ relay phase-to-ground voltage, phase Φ .
- i_Φ relay phase current, phase Φ .
- v_{TW} voltage traveling wave.
- i_{TW} current traveling wave.
- T_L line propagation time.
- P pickup of the TW87 element.

Fig. 1 presents a simplified signal acquisition diagram of our time-domain relay. We sample line currents and voltages at the rate of 1 MHz, suitable for TW protection and fault locating. We apply an analog low-pass filter to avoid signal aliasing and use a simple differentiator-smoother filter [2] to extract TWs from the raw currents and voltages. We decimate the 1 MHz samples to the 10 kHz rate for processing the incremental-quantity-based algorithms.

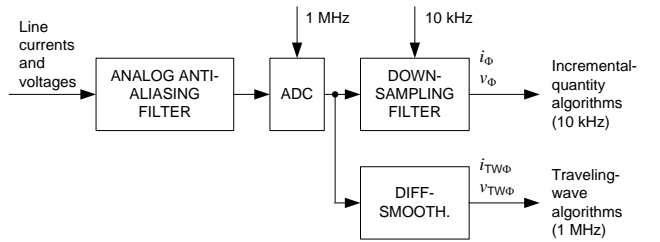


Fig. 1. Simplified data acquisition diagram for incremental-quantity and TW protection algorithms.

Fig. 2a presents the differentiator-smoother data window and Fig. 2b illustrates its operation. Considered over a period of a few tens of microseconds, the fundamental-frequency current is quasi constant (i.e., changing very slowly). A TW is a sharp change from one quasi-steady level to a different quasi-steady level. The differentiator-smoother filter responds to an ideal step change with a triangle-shaped output, and it responds to a ramp transition between two levels with a parabola-shaped output. We use the time associated with the peak of the differentiator-smoother output as the TW arrival time.

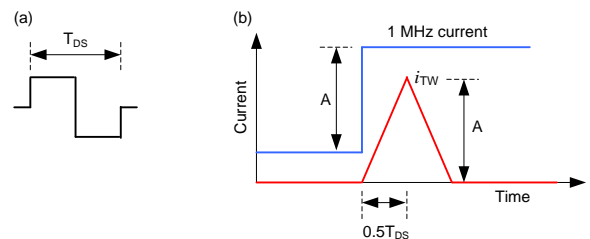


Fig. 2. Differentiator-smoother data window (a) and operation (b).

Fig. 3 depicts an integrator—a common block we use in our time-domain line protection elements. The function of an integrator is to add or accumulate input values. An integrator can be seen as a counterpart to a phasor estimator in phasor-based relays. Integrating a signal that develops from zero does not slow down decisions based on the integrated signal when comparing two or more such signals.

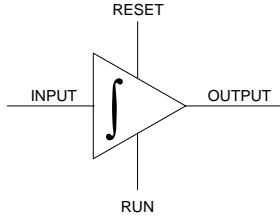


Fig. 3. Security integrator with control inputs.

In our implementation, the integrator has two control inputs (RUN and RESET) that control—via a carefully selected internal logic—its behavior under different operating conditions.

3 Traveling-wave elements

3.1 Traveling-wave directional element (TW32)

References [1] and [4] explain the fundamentals of using voltage and current TWs for fault direction discrimination. Theoretically, we need a wide-bandwidth (high-fidelity) voltage transformer to measure voltage TWs. However, in most cases, we can measure the first voltage TW even with a capacitively coupled voltage transformer, CCVT (because of interwinding capacitance across the step-down transformer and the interturn capacitance across the CCVT tuning reactor). This voltage TW measurement is not accurate in terms of voltage TW magnitude, but it is accurate in terms of the arrival time and polarity, which is sufficient for the TW32 element.

We use phase voltage and current TWs as shown in Fig. 4. We calculate the TW torque as a product of the TW current and the sign-inverted TW voltage (so the torque is positive for forward events). We integrate the torque over time. For security, we release the integrator only if both the voltage and current TWs are above minimum levels. We check the output of the integrator (E_{FWD}) after time T_1 (in the order of tens to hundreds of microseconds) from the beginning of the disturbance. We assert the TW32 output when E_{FWD} exceeds a security margin.

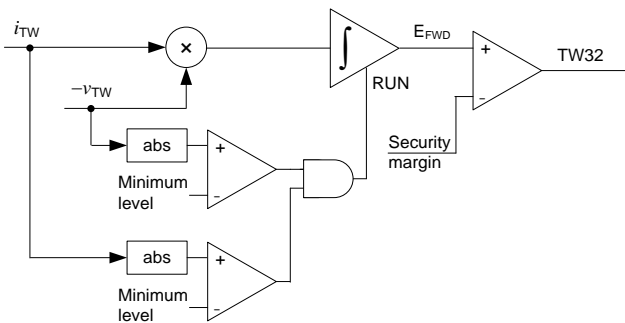


Fig. 4. Simplified logic of the TW32 element.

3.2 Traveling-wave differential element (TW87)

Reference [1] derives our TW line current differential protection principle. This element compares timing, polarities, and magnitudes of current TWs at both line terminals. For an external event, the current TW enters at one line terminal and, after the line propagation time, leaves at the other terminal with the opposite polarity but not necessarily with the same magnitude [5].

We implement the principle as follows. First, we identify the time (as a sample index) of the first TW at both the local and remote terminals. For the local and remote terminals, we label these two indices NL_{FIRST} and NR_{FIRST} , respectively. Finding these indices is not difficult because these are the first waves recorded after the quiescent steady state prior to the disturbance.

Second, knowing the index of the first TW at the local terminal, we establish a time window to detect the exiting TW at the remote terminal. Similarly, knowing the index of the first TW at the remote terminal, we establish the time window to detect the exiting TW at the local terminal. These windows are positioned at the nominal line propagation time, T_L , following the first TW. We also need to include a margin, ΔT_L , for the error and variability in the propagation time (to accommodate conditions such as conductor sagging).

Third, we inspect the TW recording in the TW exit time interval and identify the maximum absolute value in that time interval. We label the index of that maximum value identified by the local and remote relays as the exit index NL_{EXIT} and NR_{EXIT} , respectively. Fig. 5 shows the first TW at the local terminal and the exit TW at the remote terminal.

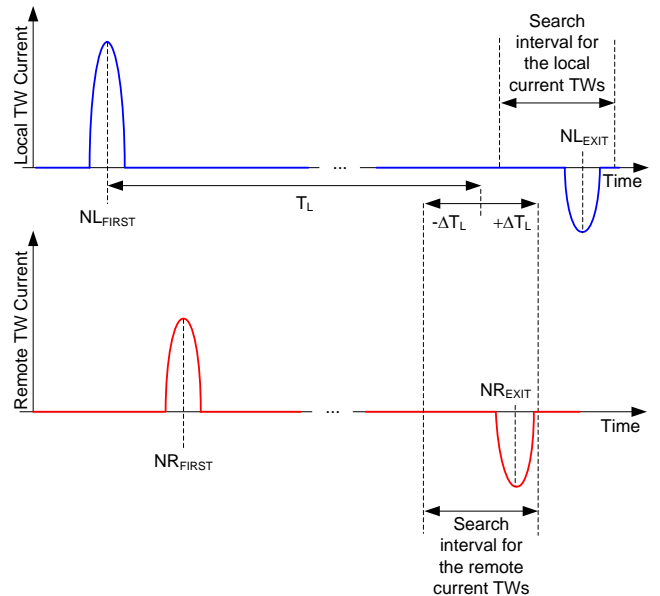


Fig. 5. Defining the FIRST and EXIT TWs for the TW87 element.

After identifying the four indices, we calculate the following signals, using M samples in the order of one half of the differentiator smoother window ($M < 0.5 \cdot T_{DS}$).

Magnitudes of the first current TWs:

$$IL = C \cdot \left| \sum_{k=-M}^{k=M} i_{TWL(NL_{FIRST}-k)} \right| \quad (1a)$$

$$IR = C \cdot \left| \sum_{k=-M}^{k=M} i_{TWR(NR_{FIRST}-k)} \right| \quad (1b)$$

We selected the scaling factor C to maintain a unity gain in the values of (1) for an ideal step TW.

Operating TW current:

$$I_{DIF} = C \cdot \left| \sum_{k=-M}^{k=M} (i_{TWL(NL_{FIRST}-k)} + i_{TWR(NR_{FIRST}-k)}) \right| \quad (2)$$

Restraining TW current:

If $NL_{FIRST} < NR_{FIRST}$,

$$I_{RST} = C \cdot \left| \sum_{k=-M}^{k=M} (i_{TWL(NL_{FIRST}-k)} - i_{TWR(NR_{EXIT}-k)}) \right| \quad (3a)$$

else,

$$I_{RST} = C \cdot \left| \sum_{k=-M}^{k=M} (i_{TWR(NR_{FIRST}-k)} - i_{TWL(NL_{EXIT}-k)}) \right| \quad (3b)$$

Fault location:

$$m_{87} = 0.5 \left(1 + \frac{NL_{FIRST} - NR_{FIRST}}{T_L} \right) \quad (4)$$

After calculating (1) through (4), we apply the TW87 logic shown in Fig. 6.

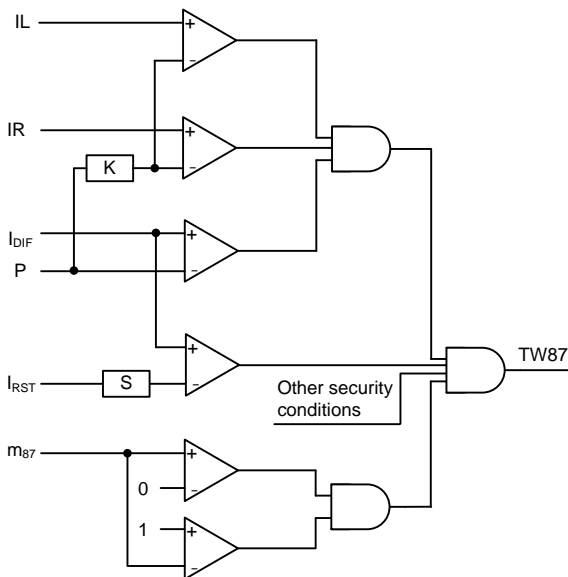


Fig. 6. Simplified TW87 logic (P–minimum pickup, S–slope, K–minimum TW factor).

We run three TW87 elements, one for each phase. Any fault type would excite at least two conductors with current TWs. For security, we require all phase elements with local, remote, and operating currents greater than their corresponding pickup level to declare an internal fault condition before we allow the TW87 to assert its output.

Any sudden voltage change at a point on the protected line launches TWs [6]. Such changes include switching in-line series capacitors and reactors or a shield wire lightning strike. Therefore, the TW87 logic requires additional supervision conditions for security. This discussion is outside the scope of this paper.

4 Incremental-quantity elements

4.1 Incremental-quantity directional element (TD32)

Reference [1] derives the theory of the TD32 element. We base the element on a torque, i.e., a product of the instantaneous incremental voltage and the instantaneous incremental replica current. We apply adaptive restraints for the operating torque using the well-known concept of the threshold impedances. We calculate the operating torque using a sign-inverted voltage so that the operating torque, T_{OP} , is positive for forward events. The two restraining torques are proportional to the product of the squared loop replica current and the corresponding threshold impedance magnitudes. We use a positive restraining torque, T_{FWD} , for checking the forward direction, and we use a negative restraining torque, T_{REV} , for checking the reverse direction. We integrate the torques (T_{OP} , T_{FWD} , T_{REV}) and compare the integrated operating torque with the adaptive integrated restraining torques and declare the forward or reverse direction.

4.2 Incremental-quantity distance element (TD21)

Reference [1] derives the theory of the TD21 element based on the fundamentals [7]. The principle compares the calculated voltage change at the intended reach point (operating voltage, V_{21OP}) with the prefault voltage at the reach point (restraining voltage, V_{21RST}). For a fault at the reach point, the highest change in the voltage is when the prefault voltage collapses all the way to zero (a bolted fault, $R_F = 0$). If the change is higher ($V_{21OP} > V_{21RST}$), the fault must be between the relay and the reach point and the element asserts.

5 Performance on time-domain line protection

In this section, we illustrate performance of time-domain line protection using both digital simulations and a selected field case.

5.1 Performance of incremental quantity elements

We used a number of real-world line faults to illustrate the operation of the time-domain line protection elements and show the difference in performance compared with traditional phasor-based protection [3]. The field cases demonstrate dependability and speed improvements. They also demonstrate security of the TD21 and TD32 elements. Each remote-end line fault is a security test for our underreaching element, and each

forward fault is a security test for our reverse-looking directional element. The tested elements operated for all line faults within their intended reach, with operating times faster by 6 to 20 ms as compared with the in-service phasor-based relays (all our cases where for 60 Hz systems).

We tested the TD21 and TD32 elements against the Zone 1 and directional elements, respectively, of two high-performance, phasor-based line protection relays A and B using data generated by an electromagnetic transient program (EMTP). We set the underreaching elements to 80 percent of the line length. All relays use solid-state trip-rated outputs.

We modeled a 161 km, 500 kV, 60 Hz line with SIR of 1.4 at both terminals. We simulated bolted faults for these tests using ten fault types and two points on wave (voltage zero and voltage peak). We modeled ideal instrument transformers in these tests.

Fig. 7 presents the operating times for the TD21 and Zone 1 elements in relays A and B. Relays A and B operate in less than a cycle for close-in faults. Both relays A and B exhibit a relatively large spread in their operating times. The TD21 element, in turn, is consistently fast with the average operating time below 4 ms.

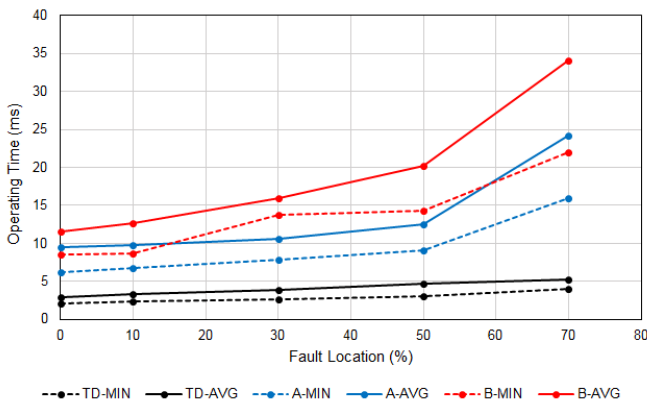


Fig. 7. Operating times of the tested underreaching elements.

Fig. 8 presents the operating times for the overreaching directional elements. Relay A operates in about half a cycle. Relay B takes 1 to 1.5 cycles to detect the fault direction. The TD32 element operates consistently in about 2 ms.

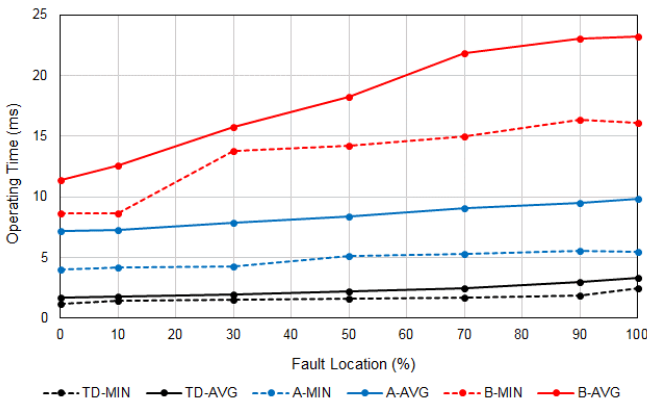


Fig. 8. Operating times of the tested directional elements.

5.2 TW32 and TW87 examples using EMTP-simulated cases

We used an EMTP to simulate an A-phase-to-ground fault at three different locations in a simple 500 kV, 60 Hz system as shown in Fig. 9. The fault resistance is zero, and the fault occurs at the voltage peak. The line length is 161 km, and the TW propagation time is 542 μ s. We simulated ideal CTs and VTs with 600:1 and 4500:1 ratios, respectively.

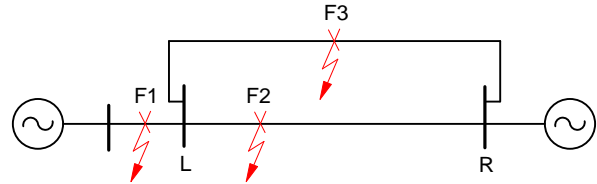


Fig. 9. Simple system for illustrating the TW32 and TW87 principles.

5.2.1 Close-in external fault F1

Fig. 10 shows the current TWs at the local and remote terminals for a close-in fault behind terminal L. As expected, the TWs measured at the L terminal with negative polarity (Phase A) are measured at the R terminal with positive polarity exactly 542 μ s later. We see the same pattern in all three phases. Table 1 lists the signals calculated from the measured TWs and used by the TW87 logic.

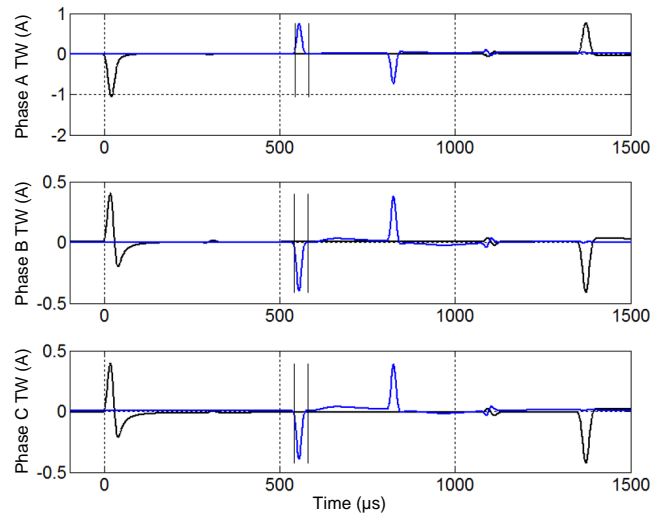


Fig. 10. Local (black) and remote (blue) current TWs for external fault F1.

For external fault F1, the TW87 algorithm calculates the operating signal well below the restraining signal (0.66 A vs. 2.16 A in Phase A, for example) and the element restrains with a large security margin.

Fig. 11 presents the A-phase voltage and current TWs at the local terminal and the integrated TW32 torque. The torque is decisively negative, and the TW32 element indicates a reverse fault direction.

Fault	Φ	I_L (A)	I_R (A)	I_{DIF} (A)	I_{RST} (A)	m_{87} (pu)
F1	A	1.41	0.75	0.66	2.16	1.0
	B	0.40	0.40	0.01	0.80	1.0
	C	0.38	0.38	0.00	0.76	1.0
F2	A	1.22	0.76	1.98	1.22	0.4
	B	0.51	0.39	0.90	0.51	0.4
	C	0.54	0.38	0.92	0.54	0.4
F3	A	0.92	0.53	1.45	1.70	0.3
	B	0.31	0.27	0.58	0.74	0.3
	C	0.30	0.28	0.57	0.72	0.3

Table 1: TW87 measurements for the EMTP examples.

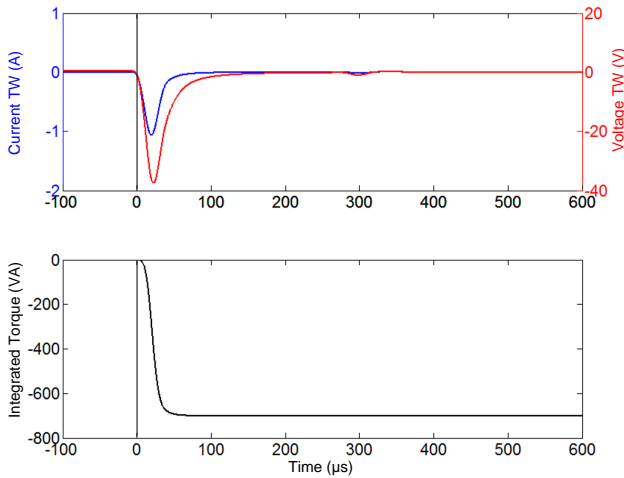


Fig. 11. Voltage and current TWs and the integrated TW32 torque at the local terminal for external fault F1.

5.2.2 Internal fault F2

Fig. 12 plots the TW87 currents for internal fault F2 at 40 percent from the local terminal. Fig. 13 plots the TW32 quantities at the local terminal. Table 1 lists the signals calculated from the measured TWs and used by the TW87 logic.

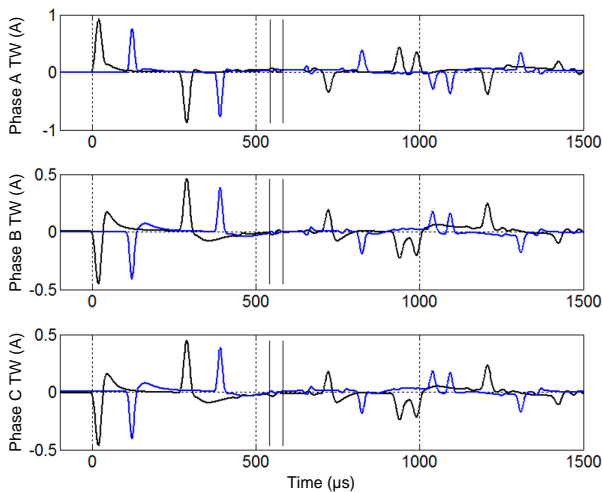


Fig. 12. Local (black) and remote (blue) current TWs for internal fault F2.

The TW87 element calculates the fault location as about 0.4 pu, and there is a very good agreement among calculations in all three phases. The TW87 operating signal is considerably above the restraining signal (1.98 A vs. 1.22 A in Phase A, for example), and the element operates dependably.

The TW32 element measures a decisively positive torque (Fig. 13) and indicates a forward fault direction dependably. The TW32 element responds in time T1 or does not respond at all. As a result, the operating time of the TW32 element, when measured from the TW arrival time at the terminal, is a constant value, well below 1 ms.

The TW87 operating time depends on the line propagation time, communications delays, and relay processing delays, as well as on fault location. We used propagation times of 0.98 and 0.6 of the speed of light in free space for the transmission line and fiber propagation velocities, respectively. We assumed 0.05 ms for the TW87 transmit and receive time delays each (using high-speed private fiber), and 0.1 ms for the logic processing time. Based on our design, for a 100 km line, the TW87 operating time is 1.2 ms.

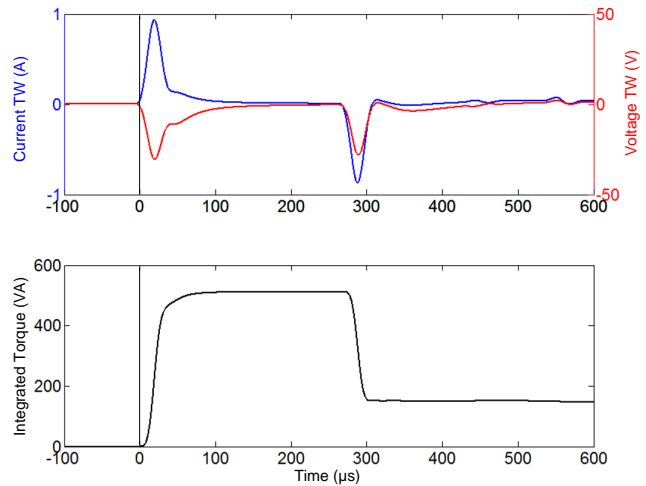


Fig. 13. Voltage and current TWs and the integrated TW32 torque at the local terminal for internal fault F2.

5.2.3 External fault F3

External fault F3 emulates a fault on a parallel path in such a way that the TWs reached the local and remote terminals at approximately the same time (the difference is less than the line propagation time) and with the same polarity. Table 1 lists the signals calculated from the measured TWs and used by the TW87 logic.

Fig. 14 shows the local and remote current TWs. The TW87 element calculates the fault location as 0.3 pu. Considering the polarities and the time difference between the first TWs recorded at each line terminal, the fault appears to be internal, located 0.3 pu from the local terminal. However, the TW87 element inspects the TWs one line propagation time past the initial waves and sees the TWs with the opposite polarity as they leave the protected line. As a result, the operating signal is lower than the restraining signal (1.45 A vs. 1.70 A in Phase A, for example), and the TW87 element restrains with a good margin.

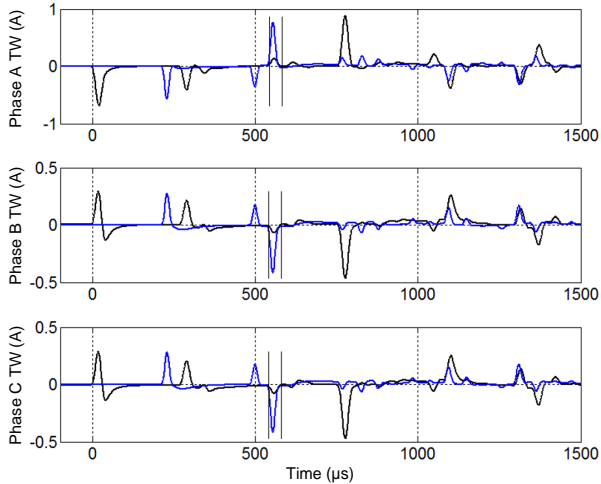


Fig. 14. Local (black) and remote (blue) current TWs for external fault F3.

5.2.4 TW87 example using field data

A B-phase-to-ground fault struck a 117 km, 161 kV line at 81 percent of the distance from the terminal. The wave propagation time measured on this line during relay commissioning is 396 μ s. These TWs have been captured and measured using the circuitry developed for the fault-locating function [1]. Nonetheless, we can use them to illustrate the TW87 principle and implementation. Fig. 15 shows the local and remote current TWs.

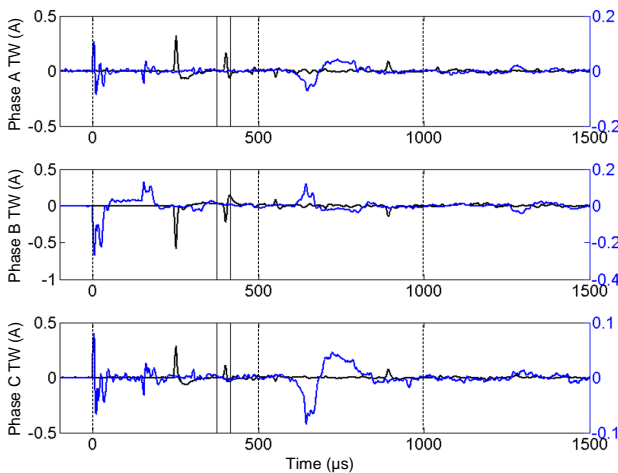


Fig. 15. Local (black) and remote (blue) current TWs captured for Cases 10 and 11.

The TW87 algorithm verifies the fault location correctly (0.798–0.811 pu calculated by m_{87} in real time vs. 0.81 pu from the TW fault locator) and operates dependably for this fault because the operating signal in Phase B is considerably higher than the restraining signal (1.03 A vs. 0.13 A).

6 Conclusions

We explained the operating principles of time-domain line protection elements: directional and distance incremental-quantity elements and differential and directional TW line current elements.

We evaluated the time-domain elements with respect to a number of factors that affect line protection performance—including fault location, system strength, and point on wave—while using two different phasor-based relays for comparison. Our testing shows the typical operating times for our time-domain line protection elements are in the order of 2 ms for the TD32, less than 1 ms for the TW32, 4 ms for the TD21, and less than 1 ms plus the channel time for the TW87 (for a 100 km line).

We intentionally biased the time-domain elements for speed and security instead of perfect dependability. Therefore, they require dependable, typically phasor-based, protection elements operating in parallel either as a part of the same relay or as a separate relay. However, these fast elements operate for a large percentage of line faults. As a result, the dependable but slower backup is called upon infrequently, resulting in excellent average operating times of the complete application.

References

- [1] E. O. Schweitzer, III, B. Kasztenny, A. Guzmán, V. Skendzic, and M. V. Mynam, “Speed of Line Protection – Can We Break Free of Phasor Limitations?” proceedings of the 41st Annual Western Protective Relay Conference, Spokane, WA, October 2014.
- [2] E. O. Schweitzer, III, A. Guzmán, M. V. Mynam, V. Skendzic, B. Kasztenny, and S. Marx, “Locating Faults by the Traveling Waves They Launch,” proceedings of the 40th Annual Western Protective Relay Conference, Spokane, WA, October 2013.
- [3] E. O. Schweitzer, III, B. Kasztenny, and M. V. Mynam, “Performance of Time-Domain Line Protection Elements on Real-World Faults,” proceedings of the 42nd Annual Western Protective Relay Conference, Spokane, WA, October 2015.
- [4] A. T. Johns, “New Ultra-High-Speed Directional Comparison Technique for the Protection of EHV Transmission Lines,” IEE Proceedings C: Generation, Transmission, and Distribution, Vol. 127, Issue 4, July 1980, pp. 228–239.
- [5] T. Takagi, J. Barbar, U. Katsuhiko, and T. Sakaguchi, “Fault Protection Based on Travelling Wave Theory, Part I: Theory,” IEEE Power Engineering Society Summer Meeting, Mexico, Paper A77, July 1977, pp. 750–753.
- [6] H. W. Dommel and J. M. Michels, “High Speed Relaying Using Traveling Wave Transient Analysis,” IEEE Power Engineering Society Winter Meeting, New York, Paper No. A78, January/February 1978, pp. 214–219.
- [7] M. Vitins, “A Fundamental Concept for High Speed Relaying,” IEEE Transactions on Power Apparatus and Systems, Vol. PAS–100, Issue 1, January 1981, pp. 163–173.